

Supplementary Information

**Mechanisms for Hydrogen Evolution on Transition Metal Phosphide Catalysts and a
Comparison to Pt(111)**

Chenyang Li,¹ Hao Gao,¹ Wan Wan,¹ and Tim Mueller,^{1,*}

¹Department of Materials Science and Engineering, Johns Hopkins University, Baltimore,
Maryland 21218, United States

*Email: tmueller@jhu.edu

DFT calculations

Density functional theory (DFT)¹ calculations were performed with the Vienna Ab initio Simulation Package (VASP),² in which the Kohn-Sham equations are solved by self-consistent algorithms. The revised Perdew-Burke-Ernzerhof (RPBE)^{3,4} exchange-correlation functional was used for all DFT calculations, as this resulted in the closest agreement with experimentally measured hydrogen adsorption energy on Pt(111) among RPBE, RPBE-D3 and PBE-D3 (Figure S1), where D3 stands for the van der Waals correction method.^{5,6} The Co, Fe, P, H_GW, Pt_pv PBE projector-augmented wave (PAW)⁷ potentials were used and all calculations were run with accurate precision with plane wave cutoff energy set to 300 eV. For all calculations with transition metal phosphides and Pt, the slab thickness and vacuum thickness were at least 10 Å and 15 Å, respectively. All atoms were allowed to relax, with hydrogen atoms symmetrically adsorbed on both sides of the slab. The Brillouin zone was sampled using efficient grids generated by the *k*-point grid server⁸ with a minimum distance of 18 Å between real-space lattice points; For Pt(111), a minimum distance of 40 Å was used. The shift vectors were automatically chosen to minimize the number of irreducible *k*-points, and the grids were automatically optimized for slab calculations. The convergence criteria for the self-consistent iteration and the ionic relaxation loop were set to 10⁻⁴ eV and 10⁻³ eV per cell, respectively.

The hydrogen adsorption free energy was calculated as $\Delta G_H = \Delta E_H + \Delta ZPE - T\Delta S$, where $\Delta E_H = E(\text{slab} + H^*) - E(\text{slab}) - \frac{1}{2}E(H_2(g))$ is the adsorption energy, ΔZPE and ΔS are the differences in zero point energy and entropy between the adsorbed H* and the H₂ gas. All ZPEs of adsorbed H* were calculated using a second-order finite difference method (normal-mode analysis) with a step size of 0.015 Å. The calculated values are shown in Table S3-S7. The *TS* of

0.41 eV/H₂ in the gas phase at 300 K was taken from the standard molecular tables.⁹ We ignored the vibrational entropy in the adsorbed state as it is generally small (0.01 eV at 300 K).^{10, 11}

The climbing image nudged elastic band^{12, 13} (CI-NEB) method was used to calculate activation barriers for the Volmer, Heyrovsky and Tafel reactions, as well as surface diffusions. For the Volmer and Heyrovsky reactions, one explicit H₂O/H₃O⁺ water layer was used. Previous work have shown little difference in the interfacial field between systems with one, two, or three water layers.^{10, 14} Molecular dynamics were run for 5 ps to obtain reasonable water structures on the phosphide surfaces. To calculate the charge transfer coefficients and the Volmer and Heyrovsky barriers at constant potential, we have applied the supercell extrapolation^{10, 14} and the charge extrapolation¹⁵ schemes by Norskov and co-workers. The atoms in the bottom two layers are fixed during relaxation, and the forces on the climbing images were converged to 0.10 eV/Å and subsequently converged to 10⁻³ eV using energy convergence. All other NEB calculations have a force convergence of 0.05 eV/Å. The zero potential used in this work is referenced to the absolute potential of 4.4 V, which has been determined experimentally.^{16, 17}

The Brønsted–Evans–Polanyi (BEP) relationships were used in the cluster expansions and Monte Carlo simulations to estimate the activation barriers for hydrogen evolution and were obtained by fitting a set of DFT-calculated activation barriers to the reaction (adsorption) energies. For the Tafel reactions the NEB calculations had difficulty converging for CoP, so we constructed the BEP relationships using the other four surfaces (Figure S4). For the Heyrovsky reactions, the BEP relationship of Pt(111) is different from that of transition metal phosphides (see Figure S5).

Cluster expansions

Cluster expansions are generalized Ising models^{18, 19} that account for many-body interactions. Here, we have used cluster expansions to model the hydrogen adsorption on transition metal phosphides and Pt surfaces. The training sets include structures with varying hydrogen coverages (0~1 ML) and supercell sizes, allowing us to use a training set of small-size supercells to construct a cluster expansion that can be used to rapidly predict the energies and atomic orders of large-size supercells as a function of temperature and applied potential. The cluster expansions included the empty cluster, the one-body clusters, all two-body clusters within a cutoff distance of 8 Å, all three-body clusters within a cutoff distance of 4 Å, and all four-body clusters within a cutoff distance of 4 Å. The effective cluster interactions (ECI) for these cluster functions were fit to the DFT training data using the Bayesian approach²⁰ with a multivariate Gaussian prior distribution for the ECI values. The prior distribution represents physical insights into the expected magnitude of the ECIs (e.g. larger clusters typically have smaller ECI). The Bayesian approach has been shown to greatly improve the predictive accuracy of the cluster expansion for a given training set size.²⁰⁻²² The inverse of the covariance matrix for the prior distribution had elements given by:

$$\lambda_{\alpha\alpha} = \begin{cases} 0, & \text{for } n_{\alpha}=0 \\ \lambda_1, & \text{for } n_{\alpha}=1 \\ \lambda_2 e^{\lambda_3 r_{\alpha}} e^{\gamma_4 n_{\alpha}}, & \text{for } n_{\alpha}>1 \end{cases} \quad (1)$$

where n_{α} is the number of sites in cluster function α , r_{α} is the cutoff distance, and parameters λ_1 , λ_2 , λ_3 , and λ_4 were determined using a conjugate gradient algorithm to minimize the leave-one-out cross validation (LOO CV) error. These final parameters are listed in Table S1. The resulting cluster expansions for Co₂P(101), CoP(101), Fe₂P(100), FeP(011), and Pt(111) have root mean square LOO CV errors of 3.4, 7.4, 7.0, 4.3, and 6.6 meV/site, respectively.

Monte Carlo simulations

Grand canonical Monte Carlo²³ simulations were performed to study the hydrogen adsorption structures and energetics as a function of temperature and applied potential. For each catalyst surface studied, simulated annealing was run from 1500 K and then decreased in steps by 50 K until 300 K. At each temperature, the number of Monte Carlo iterations was 2000 times the number of adsorption sites in the 12×12 supercell. The number of adsorption sites per unit cell for Co₂P(101), CoP(101), Fe₂P(100), FeP(011), and Pt(111) are 4, 5, 3, 4, and 2, respectively. After the annealing runs, the thermodynamically averaged current densities and hydrogen coverages were recorded during the Monte Carlo simulations at 300 K with the same iteration numbers mentioned above.

Table S1. Final fitting parameters of the cluster expansions.

	λ_1	λ_2	λ_3	λ_4
Pt	1.000E-4	9.151E-5	1.091	2.158
Co ₂ P	1.000E-4	9.053E-5	0.618	3.422
CoP	1.000E-4	8.989E-5	2.027	1.703
Fe ₂ P	1.000E-4	7.954E-5	0.790	0.639
FeP	1.000E-4	9.178E-5	1.507	2.013

Table S2. Activation barriers for the Volmer step on transition metal phosphides and Pt at 0 V. The extrapolation shows that the hydrogen deposition on Pt-top is barrierless.

	Metal site (eV)	P site (eV)
FeP	0.43	0.02
Co ₂ P	0.31	0.36
Pt	0	/

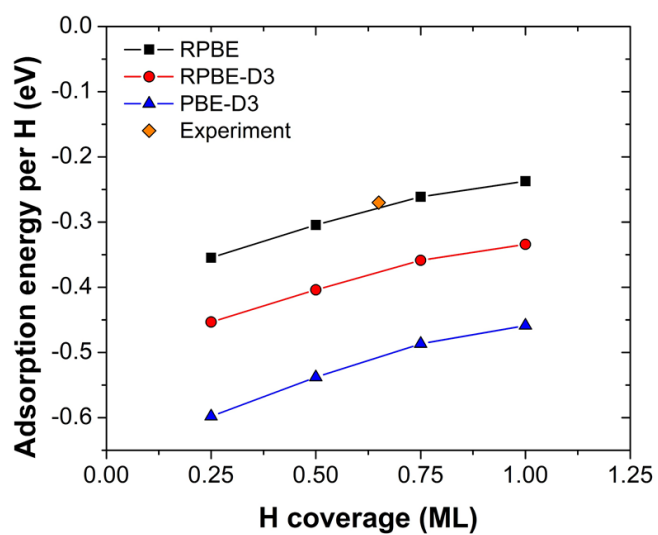


Figure S1. Comparison of hydrogen adsorption energies on Pt(111) using RPBE, RPBE-D3, and PBE-D3. The experimental value is taken from ref 5.

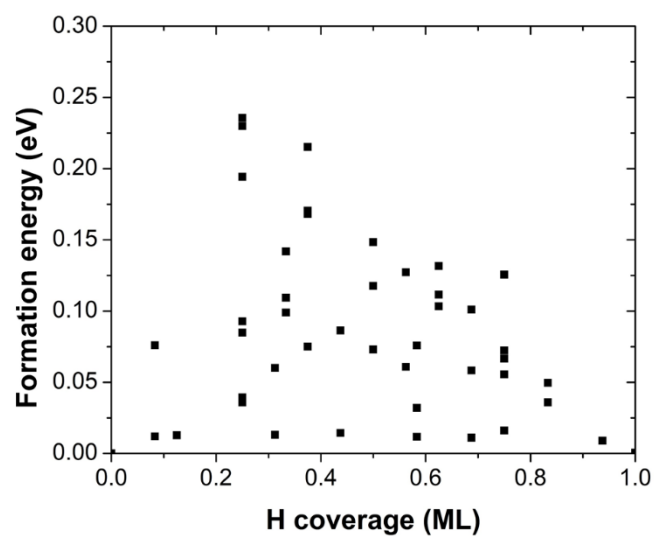
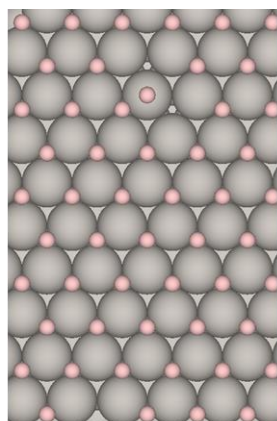
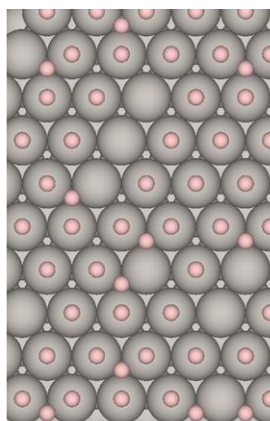


Figure S2. Training data for FeP(011). Formation energy with respect to an empty surface and a fully occupied surface.



$U = -0.16 \text{ V}$



$U = -0.18 \text{ V}$

Figure S3. Monte Carlo snapshots of hydrogen adsorption at 300 K on Pt(111) at $U = -0.16 \text{ V}$ and -0.18 V . Large grey spheres and small pink spheres represent Pt and H, respectively. A phase transition from fcc-adsorption to top-adsorption was observed when decreasing the potential.

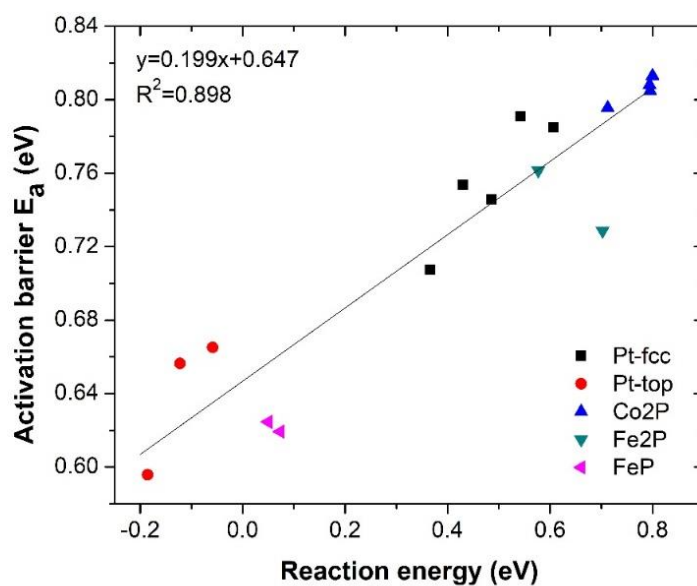


Figure S4. Brønsted–Evans–Polanyi (BEP) relationship of the Tafel reactions on Pt and transition metal phosphides. The different pairs of sites are: Pt fcc+fcc, Pt top+fcc, Co₂P Co bridge_a + bridge_a, Co₂P Co bridge_a + bridge_b, Co₂P bridge_a + P top, Fe₂P Fe bridge + bridge, Fe₂P Fe bridge + Fe-P bridge, FeP Fe bridge + bridge, FeP Fe bridge + P top.

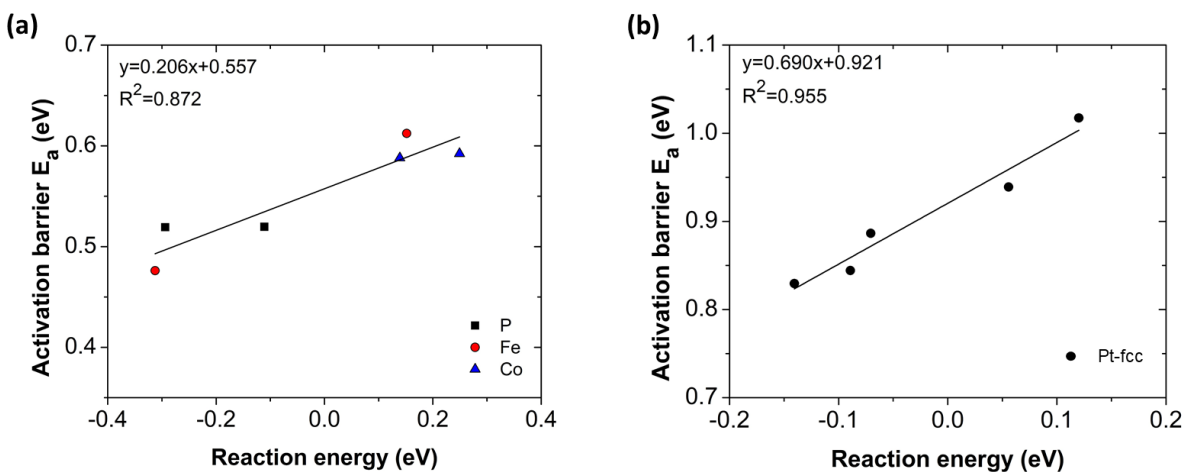


Figure S5. Brønsted–Evans–Polanyi (BEP) relationship of the Heyrovsky reactions at 0 V on (a) transition metal phosphides and (b) Pt fcc sites with different hydrogen coverages. The sites on transition metal phosphides are: P sites of CoP and FeP, Fe sites of FeP and Fe₂P, Co bridge_*a* sites of Co₂P (one with dilute coverage and one with nearby Co bridge_*b* site occupied). All other sites on transition metal phosphides are with dilute coverage.

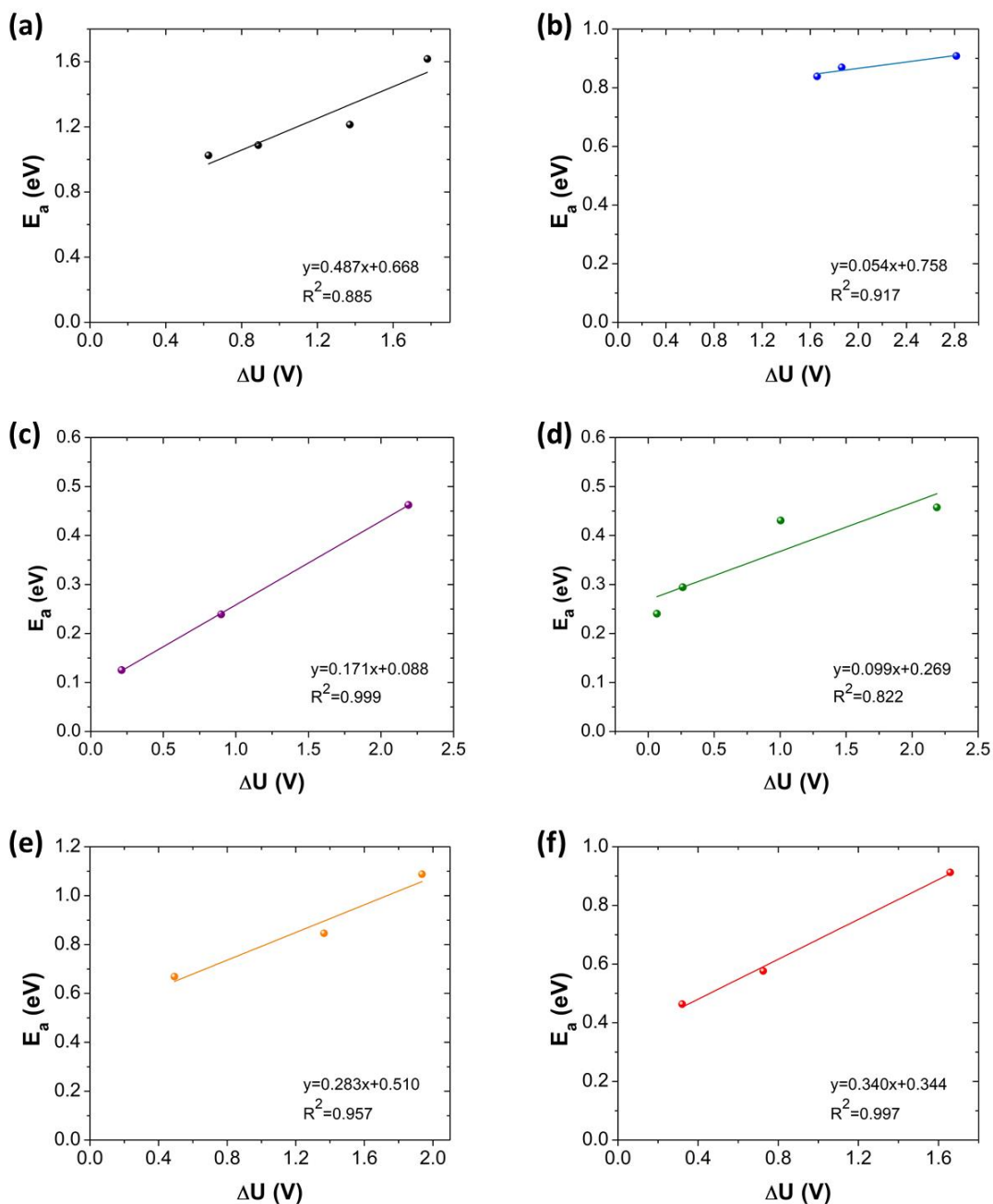


Figure S6. DFT-calculated Heyrovsky activation barriers E_a on (a) fcc site of Pt, (b) P site of FeP, (c) Fe site of Fe₂P, (d) P site of CoP, (e) Fe site of FeP, and (f) Co bridge_a site of Co₂P by using the supercell extrapolation scheme.^{10, 14} ΔU is the change in potential between the initial state (with H*) and final state (with H₂). Charge transfer coefficients are obtained as the slopes of the linear fits.

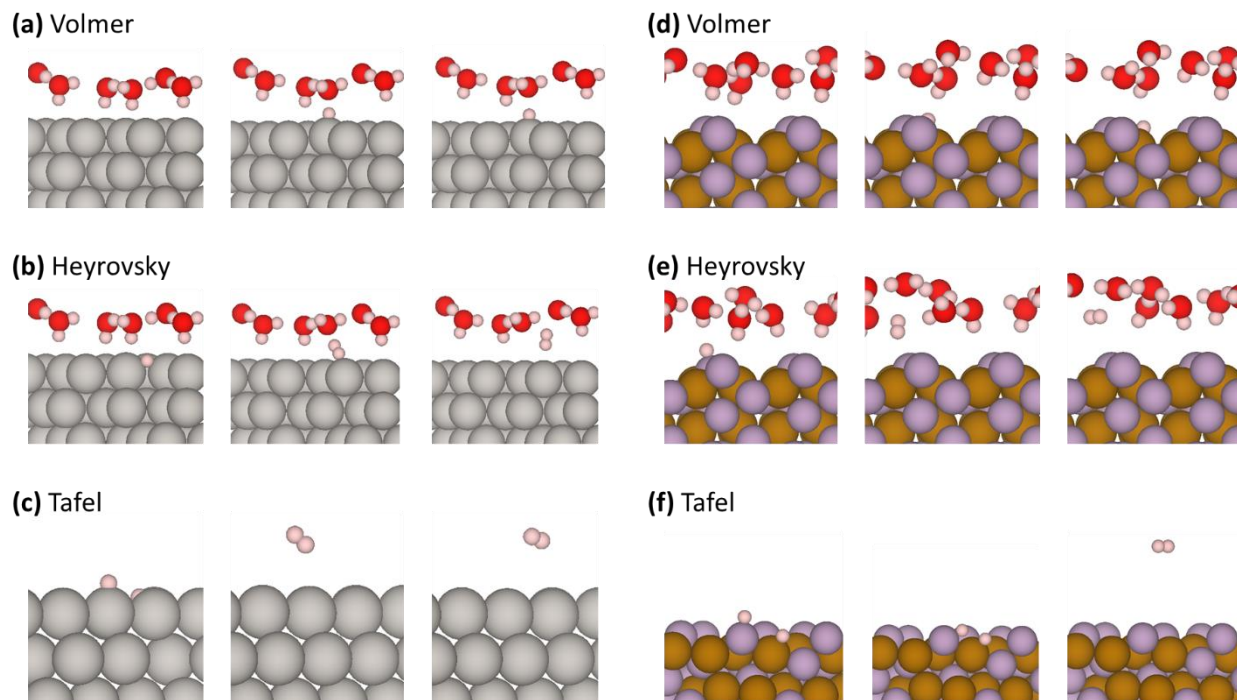


Figure S7. Elementary steps of Volmer, Heyrovsky and Tafel reactions on (a-c) Pt and (d-f) FeP. The columns within each panel correspond the initial state, transition state, and final state. Grey spheres represent Pt, gold spheres represent Fe, purple spheres represent P, red spheres represent O, and pink spheres represent H.

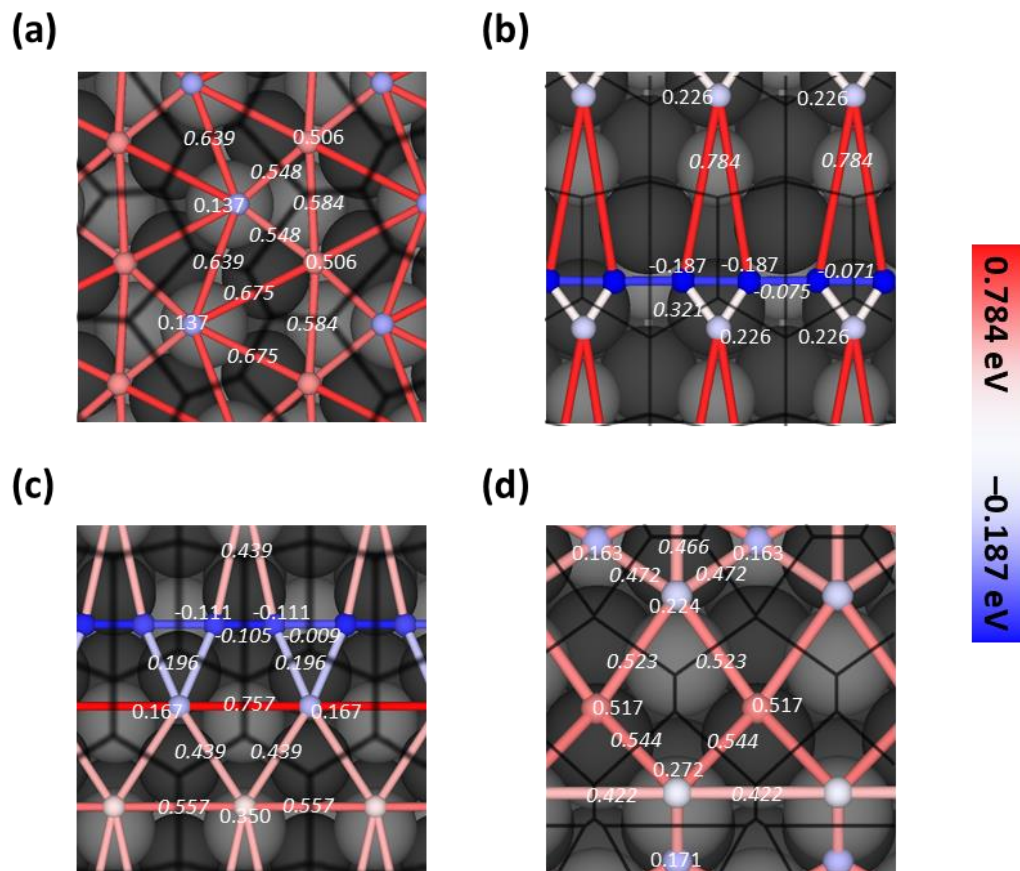


Figure S8. DFT-calculated hydrogen diffusion paths and barriers on (a) FeP, (b) Fe₂P, (c) Co₂P, and (d) CoP. Large grey and black spheres are the P and metal atom of the underlying material. Small spheres are H atoms. The color of the small hydrogen atom (and number) indicates the adsorption energy in eV at the specific site, and the color of the bond between two hydrogen atoms indicates the transition state energy along this path (given by numbers in italics). The black lines indicate the edges on the Voronoi diagrams that define neighboring atoms.

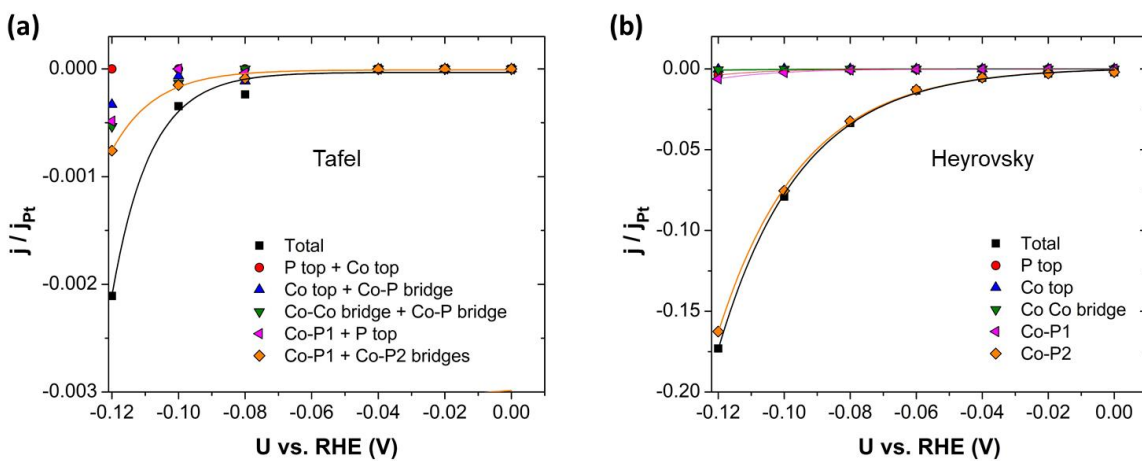


Figure S9. HER current density of CoP(101) as a function of applied potential assuming the rate-limiting step is either a Tafel reaction (a), or a Heyrovsky reaction (b). The current density is expressed as relative current to the Tafel current of Pt(111), which is denoted as j_{Pt} .

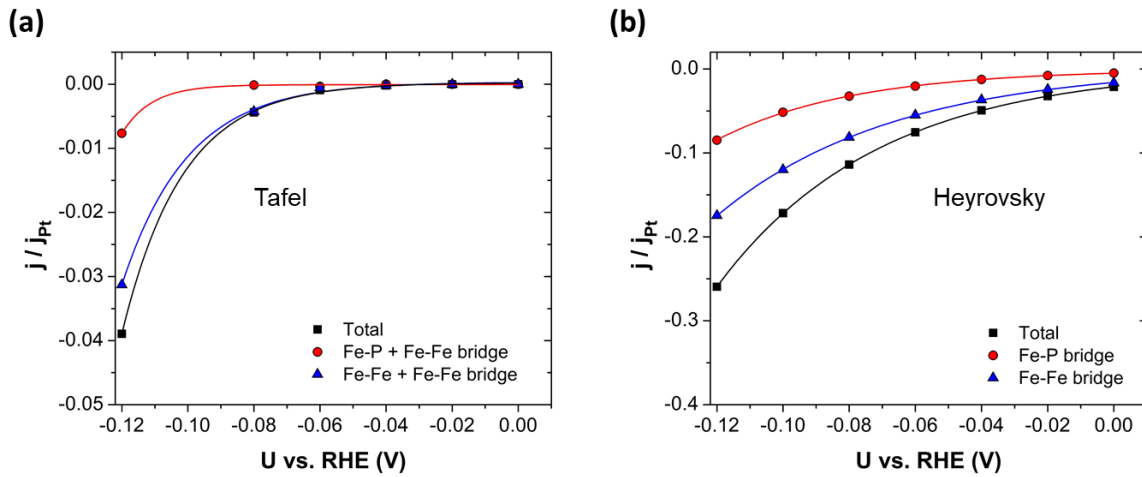


Figure S10. HER current density of Fe₂P(100) as a function of applied potential assuming the rate-limiting step is either a Tafel reaction (a), or a Heyrovsky reaction (b). The current density is expressed as relative current to the Tafel current of Pt(111), which is denoted as j_{Pt} .

Table S3. Zero point energies (ZPE) of hydrogen adsorption on Co₂P.

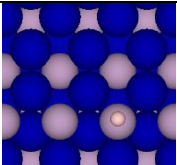
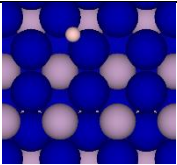
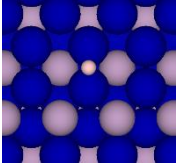
	ZPE (eV)	
P-top	0.139	
Co-Co bridge_ <i>a</i>	0.146	
Co-Co bridge_ <i>b</i>	0.082	

Table S4. Zero point energies (ZPE) of hydrogen adsorption on CoP.

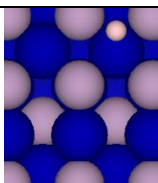
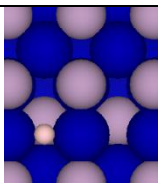
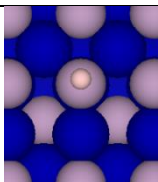
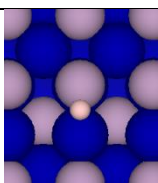
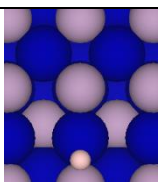
	ZPE (eV)	
Co-top	0.115	
Co-Co bridge	0.138	
P-top	0.140	
Co-P1	0.177	
Co-P2	0.147	

Table S5. Zero point energies (ZPE) of hydrogen adsorption on Fe₂P.

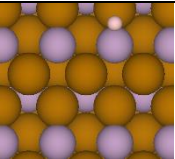
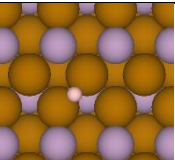
	ZPE (eV)	
Fe-P bridge	0.165	
Fe-Fe bridge	0.168	

Table S6. Zero point energies (ZPE) of hydrogen adsorption on FeP.

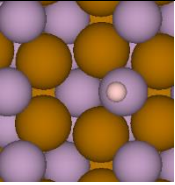
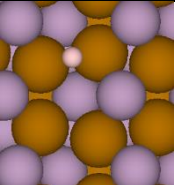
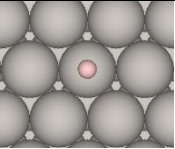
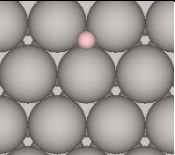
	ZPE (eV)	
P-top	0.142	
Fe-Fe bridge	0.139	

Table S7. Zero point energies (ZPE) of hydrogen adsorption on Pt.

	ZPE (eV)	
Pt-top	0.188	
Pt-fcc	0.121	

References

1. W. Kohn and L. J. Sham, *Physical Review*, 1965, **140**, A1133-A1138.
2. G. Kresse and J. Furthmüller, *Physical Review B*, 1996, **54**, 11169-11186.
3. B. Hammer, L. B. Hansen and J. K. Nørskov, *Physical Review B*, 1999, **59**, 7413-7421.
4. J. P. Perdew, K. Burke and M. Ernzerhof, *Phys. Rev. Lett.*, 1996, **77**, 3865-3868.
5. R. Gómez, J. M. Orts, B. Álvarez-Ruiz and J. M. Feliu, *The Journal of Physical Chemistry B*, 2004, **108**, 228-238.
6. S. Grimme, J. Antony, S. Ehrlich and H. Krieg, *The Journal of Chemical Physics*, 2010, **132**, 154104.
7. P. E. Blöchl, *Physical Review B*, 1994, **50**, 17953-17979.
8. P. Wisesa, K. A. McGill and T. Mueller, *Physical Review B*, 2016, **93**, 155109.
9. P. W. Atkins, *Physical chemistry*, Oxford University Press, Oxford; Melbourne; Tokyo, 1998.
10. E. Skúlason, V. Tripkovic, M. E. Björketun, S. Gudmundsdottir, G. Karlberg, J. Rossmeisl, T. Bligaard, H. Jónsson and J. K. Nørskov, *J. Phys. Chem. C*, 2010, **114**, 18182-18197.
11. J. K. Nørskov, T. Bligaard, A. Logadottir, J. R. Kitchin, J. G. Chen, S. Pandalov and U. Stimming, *J. Electrochem. Soc.*, 2005, **152**, J23-J26.
12. G. Henkelman, B. P. Uberuaga and H. Jónsson, *The Journal of Chemical Physics*, 2000, **113**, 9901-9904.
13. G. Henkelman and H. Jónsson, *The Journal of Chemical Physics*, 2000, **113**, 9978-9985.
14. J. Rossmeisl, E. Skúlason, M. E. Björketun, V. Tripkovic and J. K. Nørskov, *Chem. Phys. Lett.*, 2008, **466**, 68-71.
15. K. Chan and J. K. Nørskov, *The Journal of Physical Chemistry Letters*, 2015, **6**, 2663-2668.
16. S. Trasatti, in *Pure Appl. Chem.* 1986, vol. 58, p. 955.
17. J. E. B. Randles, *Transactions of the Faraday Society*, 1956, **52**, 1573-1581.
18. E. Ising, *Zeitschrift für Physik*, 1925, **31**, 253-258.
19. J. M. Sanchez, F. Ducastelle and D. Gratias, *Physica A: Statistical Mechanics and its Applications*, 1984, **128**, 334-350.
20. T. Mueller and G. Ceder, *Physical Review B*, 2009, **80**, 024103.
21. T. Mueller, *Physical Review B*, 2012, **86**, 144201.
22. L. Cao, C. Li and T. Mueller, *Journal of Chemical Information and Modeling*, 2018, **58**, 2401-2413.
23. N. Metropolis, A. W. Rosenbluth, M. N. Rosenbluth, A. H. Teller and E. Teller, *The Journal of Chemical Physics*, 1953, **21**, 1087-1092.